Journal of Power Sources 246 (2014) 808–818

Contents lists available at ScienceDirect

Journal of Power Sources

journal homepage: www.elsevier.com/locate/jpowsour

Thermal and energy battery management optimization in electric vehicles using Pontryagin's maximum principle

Sebastian Bauer*, Andre Suchaneck, Fernando Puente León

Institute of Industrial Information Technology, Karlsruhe Institute of Technology (KIT), Hertzstrasse 16, 76187 Karlsruhe, Germany

HIGHLIGHTS

- Batteries in electric vehicles should be operated within a narrow temperature range.
- Tempering requires electric energy that has to be provided by the battery.
- Optimization managing both demands is conducted using Pontryagin's maximum principle.
- A causal tempering strategy is derived from the optimization results.
- This tempering strategy can be applied to batteries not only in electric vehicles.

ARTICLE INFO

Article history:
Received 7 March 2013
Received in revised form
25 July 2013
Accepted 6 August 2013
Available online 15 August 2013

Keywords:
Optimal control
Energy management
Thermal management
Electric vehicle
Battery aging
Pontryagin's principle

ABSTRACT

Depending on the actual battery temperature, electrical power demands in general have a varying impact on the life span of a battery. As electrical energy provided by the battery is needed to temper it, the question arises at which temperature which amount of energy optimally should be utilized for tempering. Therefore, the objective function that has to be optimized contains both the goal to maximize life expectancy and to minimize the amount of energy used for obtaining the first goal. In this paper, Pontryagin's maximum principle is used to derive a causal control strategy from such an objective function. The derivation of the causal strategy includes the determination of major factors that rule the optimal solution calculated with the maximum principle. The optimization is calculated offline on a desktop computer for all possible vehicle parameters and major factors. For the practical implementation in the vehicle, it is sufficient to have the values of the major factors determined only roughly in advance and the offline calculation results available. This feature sidesteps the drawback of several optimization strategies that require the exact knowledge of the future power demand. The resulting strategy's application is not limited to batteries in electric vehicles.

1. Introduction

At the moment, extended research is being conducted on fuel cell, hybrid electric and pure electric vehicles [1–3]. In this paper, the focus is put on electric vehicles.

Although historians still argue who invented the very first electric vehicle, electric vehicles had been invented as early as in the first half of the 19th century. A brief history summary is given in [4,5]. Despite its early invention date, electric vehicles were superseded by internal combustion engine vehicles at the beginning of the 20th century. The reasons for this supersession were mainly technical ones: the short range and low top speed of the electric vehicle which were linked to the poor battery storage capacity. Due to slow progress in battery technology and high battery prices resulting in high vehicle prices, internal combustion engine vehicles outperformed electric vehicles [5].

Nowadays, the limited availability of fossil fuels and the greenhouse effect make it necessary to further investigate low-emission or preferably emission-free propulsion systems that do not depend on fossil fuels. This leads to a revival of electric vehicle technology and extended research in this field. Still, the factors hindering the widespread use of electric vehicles are mainly the same as back then and are related to the battery characteristics and performance: even lithium-ion batteries, considered the best available batteries on the market, feature only low energy density, leading to short range and high weight [2,4,6,7]. Additionally, they are rather expensive [8,9]. All these characteristics even of the best

* Corresponding author. Tel.: +49 (0)721 608 44515; fax: +49 (0)721 608 44500.
E-mail addresses: sebastian.bauer@kit.edu (S. Bauer), suchaneck@kit.edu (A. Suchaneck), puente@kit.edu (F. Puente León).

0378-7753/$ – see front matter © 2013 Elsevier B.V. All rights reserved.
http://dx.doi.org/10.1016/j.jpowsour.2013.08.020

available batteries make it necessary to use an intelligent battery thermal and energy management system [10]. Among other tasks [10], battery management systems in general contribute to optimally using the stored electric energy and preserving the battery, increasing its life expectancy. The thrifty use of the stored energy makes it possible to decrease the required battery capacity and/or increase the vehicle range, whereas increasing the life expectancy ensures long life of the investment.

As electric vehicles have an electric machine and a battery, regenerative braking is possible. This fact enables electric vehicles to come along with less energy than, e.g., combustion engine vehicles because these cannot store and re-apply the energy generated by the regenerative braking process. Due to the fact that the battery can be charged with electricity from renewable resources, even CO_2-free propulsion is possible.

Apart from the electrical aspect, the battery life span also has to be considered. Major factors influencing the rate of battery aging are temperature, depth of discharge and discharge rate. [11] considers these factors for $LiFePO_4$ cells. The discharge rate will not be considered in this paper, because it is defined by the driver's demand, which should be fulfilled. Time effects on the battery during storage are also neglected, as these cannot be affected as well. The same electric power demand has a varying impact on the battery life expectancy depending on the actual battery temperature [9,12]. For physical effects in the battery causing degradation, see e.g., [13]. Because of the temperature effects impacting battery aging, it makes sense to heat or cool the battery to operate it in a gentle temperature range. An optimal strategy has to be found to balance both the requirements energy saving and mild battery usage. The need for such an optimal strategy motivates the use of optimization techniques. Optimization techniques have been applied to various tasks in the field of automotive technology: to hybrid electric vehicle power management (i.e., the power split between combustion engine/fuel cell and electric motor) [14], component sizing [14] and battery thermal performance optimization in electric vehicles [15], to name a few. Examples of optimization tools are fuzzy logic [16], neural networks [17], heuristic rules [18] and deterministic methods. A very powerful deterministic tool, finding the global optimum with respect to the used value discretization, is dynamic programming (DP) [19,20]. It provides the optimal input needed to reach optimal system behavior. Though it is reasonable to go for the global optimum, the major disadvantage of DP is the huge computational effort that has to be taken to find it [19]. A deterministic alternative also capable of finding the globally optimal solution is Pontryagin's maximum principle (PMP) [21]. PMP (or its dual formulation, Pontryagin's minimum principle) has been applied successfully to various engineering problems in automotive technology, e.g., to the power split problem in hybrid electric vehicles [21–23] or to finding an optimal cold startup strategy for plug-in hybrid electric vehicles [24]. It provides necessary conditions for finding the optimum. In some cases, these can be even sufficient. The application of PMP is comparatively convenient due to the fact that it requires the solution of differential equations rather than calculating all possible solutions as with the brute-force DP approach. DP is able to easily involve state constraints, but these are not required by the present problem.

Both DP and PMP require the whole driving cycle to be known before starting the optimization process. Section 6 addresses this drawback. It identifies the main parameters of the driving cycle that have to be known instead of its detailed variation in time. With these parameters, a close-to-optimal, causal strategy derived from the PMP optimization results is applicable.

The intention behind the present work is to abstract detailed models of, e.g., battery and battery tempering to system level, where the reasonable use of PMP is enabled. For a detailed description of lithium-ion batteries, e.g., the spatial distribution of temperature and current density, we refer to [25,26]. Neglecting specific effects results in a lack of accuracy, but in turn, key factors greatly impacting the optimization can be identified. Fig. 18 at the very end of this paper shows a comparison between PMP and DP. For the PMP optimization, it is assumed that battery resistance and open-circuit voltage are constant and do not depend on state-of-charge and battery temperature, whereas during the DP optimization, the dependence is involved. The outcome of the PMP optimization is mainly governed by the initial temperature, not by the values of the aforementioned two parameters, see also Section 6. Both PMP and DP optimization results hardly differ, indicating that the simplifications can be made without a significant loss in accuracy.

Starting from the battery's system model described in Section 2, it will be shown that no formal solution of the PMP optimization (Section 3) applied to the given problem could be found. Still, the problem can be solved numerically, see Section 4. From the results of the numerical solution, presented in Section 5, a generally applicable, causal solution is derived in Section 6.

2. Battery system model

To solve the optimization problem, the battery has to be modeled electrically and thermally. The electric system model of the battery consists of a voltage source with its internal resistance connected in series, see Fig. 1 [27]. The model is also used in similar system level optimization scenarios, e.g., [9]. When it is evident from the context, the argument (t) will be omitted in the following. The open-circuit voltage U_{oc} depends on the current state-of-charge SOC, while the internal resistance $R_{bat}(SOC,\vartheta)$ is a function of both SOC and the battery temperature ϑ. The terminal voltage U_{bat} is calculated by

$$U_{bat} = U_{oc} - I_{bat}R_{bat}. \tag{1}$$

The equation for the battery current I_{bat} is

$$I_{bat} = \frac{P_{trac} + P_{temp} + P_{aux}}{U_{bat}}, \tag{2}$$

where P_{trac} stands for the demanded traction power, while P_{temp} is the electric power that is needed to temper the battery. P_{aux} is the power required by auxiliary consumer loads other than the battery tempering system. As both P_{trac} and P_{aux} are time-dependent system parameters, they can be merged into P_{trac}. In this paper, P_{aux} is assumed to be zero. Eqs. (1) and (2) combine to

$$I_{bat} = \frac{U_{oc} - \sqrt{U_{oc}^2 - 4R_{bat}(P_{trac} + P_{temp})}}{2R_{bat}}. \tag{3}$$

Only the negative root is considered due to the fact that an increased power demand requires a higher battery current. The state-of-charge SOC is defined by the ratio between currently stored charge $C(t)$ and nominal capacity C_{nom},

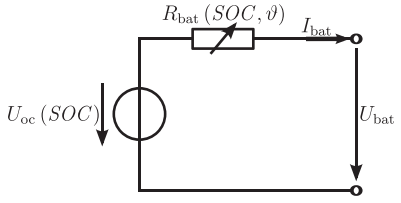

Fig. 1. Battery equivalent circuit diagram.

$$\mathrm{SOC}(t) = \frac{C(t)}{C_{\mathrm{nom}}}. \tag{4}$$

Using Eq. (2), the derivative of the state-of-charge in Eq. (4) is expressed by

$$\dot{\mathrm{SOC}}(t) = \frac{\dot{C}(t)}{C_{\mathrm{nom}}} = \frac{I_{\mathrm{bat}}(t)}{C_{\mathrm{nom}}}. \tag{5}$$

The convention that current discharging the battery is positive leads to

$$\begin{aligned}\dot{\mathrm{SOC}}(t) &= -\frac{I_{\mathrm{bat}}}{C_{\mathrm{nom}}} \\ &= \frac{\sqrt{U_{\mathrm{oc}}^2 - 4R_{\mathrm{bat}}\left(P_{\mathrm{trac}}+P_{\mathrm{temp}}\right)} - U_{\mathrm{oc}}}{2R_{\mathrm{bat}}C_{\mathrm{nom}}}.\end{aligned} \tag{6}$$

Thermally, the battery is described as lumped mass with heat capacity $C_{\mathrm{th,bat}}$. This leads to the following equation for the battery temperature ϑ:

$$\begin{aligned}\dot{\vartheta}(t) &= \frac{1}{C_{\mathrm{th,bat}}}\left(I_{\mathrm{bat}}^2 R_{\mathrm{bat}} + \dot{Q}_{\mathrm{amb}} + \dot{Q}\right) \\ &= \frac{\frac{\left(U_{\mathrm{oc}} - \sqrt{U_{\mathrm{oc}}^2 - 4(P_{\mathrm{trac}}+P_{\mathrm{temp}})R_{\mathrm{bat}}}\right)^2}{4R_{\mathrm{bat}}} + \dot{Q} + \dot{Q}_{\mathrm{amb}}}{C_{\mathrm{th,bat}}}.\end{aligned} \tag{7}$$

In Eq. (7), $\dot{Q}_{\mathrm{amb}}$ is the heat emission to the environment while the variable $\dot{Q}$ is the heat power transferred to the coolant.

The electric power P_{temp} only accounts for the electric power necessary to produce the heat flow rate $\dot{Q}$ at the battery.

The traction power P_{trac} for plain road is calculated from the given velocity v by [28]

$$P_{\mathrm{trac}} = \begin{cases} \left(v\left(F_{\mathrm{r}} + F_{\mathrm{a}} + \frac{1}{2}mv^2\right)\right)/\eta, & \text{propelling} \\ \left(v\left(F_{\mathrm{r}} + F_{\mathrm{a}} + \frac{1}{2}mv^2\right)\right)\cdot\eta, & \text{braking.} \end{cases} \tag{8}$$

F_{r} is the (velocity dependent) resistance to rolling, F_{a} the (velocity dependent) aerodynamic drag. m stands for the vehicle mass, η is the traction system efficiency factor. It depends on both torque and rotational speed. For a given driving cycle providing the vehicle speed, the required traction power is calculated offline.

3. Pontryagin's maximum principle

Pontryagin's maximum principle (PMP) is of outstanding importance in the field of optimal control. It provides necessary conditions for the calculation of the optimal system input that minimizes a given objective function. It has been applied successfully to the power-split problem between internal combustion engine and electric motor in hybrid vehicles, see, e.g., [29].

In the following, the optimal values for input, state and costate variables will be indicated with the superscript o. For a detailed description on the dual minimum principle, see [30]. The PMP is applied to a nonlinear, time-variant state space model,

$$\dot{\mathbf{x}}(t) = f(\mathbf{x}(t), \mathbf{u}(t), t), \tag{9}$$

where $\mathbf{x}(t)$ is the state vector and $\mathbf{u}(t)$ the input vector. It uses the boundary conditions

$$\mathbf{x}(t_0) = \mathbf{x}_0, \tag{10}$$

$$\mathbf{x}(t_{\mathrm{e}}) = \mathbf{x}_{\mathrm{e}} \tag{11}$$

and the objective function

$$J = h(\mathbf{x}(t_{\mathrm{e}}), t_{\mathrm{e}}) + \int_{t_0}^{t_{\mathrm{e}}} f_0(\mathbf{x}(t), \mathbf{u}(t), t)\mathrm{d}t. \tag{12}$$

The PMP then provides necessary conditions for the calculation of the optimal system input $\mathbf{u}(t)$ that minimizes the objective function (12). t_0 is the beginning of the considered time interval, while t_{e} is its end point. Using the definition of the Hamiltonian

$$H(\mathbf{x}, \boldsymbol{\psi}, \mathbf{u}, t) = -f_0(\mathbf{x}, \mathbf{u}, t) + \boldsymbol{\psi}^{\top} f(\mathbf{x}, \mathbf{u}, t), \tag{13}$$

the necessary conditions are

$$\dot{\mathbf{x}}^{\mathrm{o}} = \left.\frac{\partial H}{\partial \boldsymbol{\psi}}\right|_{\mathrm{o}} = f(\mathbf{x}^{\mathrm{o}}(t), \mathbf{u}^{\mathrm{o}}(t), t), \tag{14a}$$

$$\dot{\boldsymbol{\psi}}^{\mathrm{o}} = -\left.\frac{\partial H}{\partial \mathbf{x}}\right|_{\mathrm{o}}, \tag{14b}$$

$$H(\mathbf{x}^{\mathrm{o}}, \boldsymbol{\psi}^{\mathrm{o}}, \mathbf{u}^{\mathrm{o}}, t) \overset{!}{\rightarrow} \max_{\mathbf{u}\in S}, \tag{14c}$$

$$\mathbf{x}^{\mathrm{o}}(t_0) = \mathbf{x}_0, \tag{14d}$$

$$\mathbf{x}^{\mathrm{o}}(t_{\mathrm{e}}) = \mathbf{x}_{\mathrm{e}}. \tag{14e}$$

The last condition (14e) is only applicable when the end value $\mathbf{x}_{\mathrm{e}}$ is given and fix. For a free end value, the transversality condition

$$\boldsymbol{\psi}^{\mathrm{o}}(t_{\mathrm{e}}) = -\left.\left(\frac{\partial h}{\partial \mathbf{x}}\right)\right|_{\mathrm{o},t_{\mathrm{e}}} \tag{15}$$

has to be fulfilled. The vector ψ is the costate vector; each state has a corresponding costate. Eq. (14c) is called control equation and yields the optimal input $\mathbf{u}^{\mathrm{o}}$. As not all values for $\mathbf{u}^{\mathrm{o}}$ that are calculated by the PMP are feasible (for example, one or more inputs are bounded), S in Eq. (14c) is the subspace of $\mathbb{R}^p$ ($p = \dim(\mathbf{u})$) which contains the valid values of $\mathbf{u}$.

4. Optimization using Pontryagin's maximum principle

The following arguments will be omitted for the rest of this paper when their presence is clear from the context:

$$\begin{aligned} \mathrm{SOC} &= \mathrm{SOC}(t) & P_{\mathrm{temp}} &= P_{\mathrm{temp}}\left(\dot{Q}(t)\right) \\ \vartheta &= \vartheta(t) & P_{\mathrm{trac}} &= P_{\mathrm{trac}}(t) \\ U_{\mathrm{oc}} &= U_{\mathrm{oc}}(\mathrm{SOC}(t)) & \psi_1 &= \psi_1(t) \\ R_{\mathrm{bat}} &= R_{\mathrm{bat}}(\mathrm{SOC}(t),\ \vartheta(t)) & \psi_2 &= \psi_2(t) \\ \dot{Q} &= \dot{Q}(t) & H &= H(\mathbf{x}, \boldsymbol{\psi}, \mathbf{u}, t) \\ \dot{Q}_{\mathrm{amb}} &= \dot{Q}_{\mathrm{amb}}(t). \end{aligned}$$

4.1. Pontryagin's maximum principle applied to the system model

As mentioned before, the goal of the optimization is to find a strategy which operates the battery preferably within a temperature range in which it is stressed least, while at the same time the amount of electrical energy needed to temper the battery appropriately is minimized. This leads to the objective function

$$J = \int_{t_0}^{t_{\mathrm{e}}} \left(-\dot{\mathrm{SOC}} + w_1 \lambda(\vartheta)\right)\mathrm{d}t. \tag{16}$$

In Eq. (16), the integral of $-\dot{\mathrm{SOC}}$ means that the SOC at the end time has to be as high as possible. $\lambda(\vartheta)$ is a mathematical quantity that describes the influence of temperature on the battery life; the higher its value, the more the battery is stressed. w_1 is the

weighting coefficient between both effects. Its value results from the provided requirements on the battery life span dependent on the operational demands, i.e., while undergoing a certain driving cycle a fixed number of times, the battery has to last a predefined time period. From the objective function (16), the rate of heat flow $\dot{Q}(t)$ (system input) that minimizes its value has to be determined. Substituting Eq. (6) in Eq. (16) results in

$$J = \int_{t_0}^{t_e} \frac{U_{oc} - \sqrt{U_{oc}^2 - 4(P_{trac} + P_{temp})R_{bat}}}{2C_{nom}R_{bat}} + w_1\lambda(\vartheta)\mathrm{d}t. \tag{17}$$

Therefore, the Hamiltonian for this optimization problem is

$$\begin{aligned} H = &-\frac{U_{oc} - \sqrt{U_{oc}^2 - 4(P_{trac} + P_{temp})R_{bat}}}{2C_{nom}R_{bat}} - w_1\lambda(\vartheta) \\ &- \frac{\psi_1\left(U_{oc} - \sqrt{U_{oc}^2 - 4(P_{trac} + P_{temp})R_{bat}}\right)}{2C_{nom}R_{bat}} \\ &+ \frac{\psi_2\left(\frac{\left(U_{oc} - \sqrt{U_{oc}^2 - 4(P_{trac}+P_{temp})R_{bat}}\right)^2 + \dot{Q} + \dot{Q}_{amb}}{4R_{bat}}\right)}{C_{th,bat}}. \end{aligned} \tag{18}$$

Considering the fact that the battery can be heated or cooled, the relation between $\dot{Q}$ and P_{temp} is defined linearly by

$$P_{temp}\left(\dot{Q}\right) := \begin{cases} a_h \cdot \dot{Q} & \text{for } \dot{Q} \geq 0 \\ a_c \cdot \dot{Q} & \text{for } \dot{Q} < 0 \end{cases}; \quad a_h > 0, a_c < 0, \tag{19}$$

since for both heating ($\dot{Q} \geq 0$) and cooling ($\dot{Q} < 0$), a positive amount of electric energy has to be provided by the battery. It has to be made sure by higher-level systems that the total requested power can be delivered by the battery. The exact shape of relation (19) mainly depends on the used tempering system. Due to the generic character of this paper, however, it is beyond its scope to investigate characteristics of different systems, and thus, linear dependence is assumed.

Keeping in mind that the investigated system has two states, state-of-charge SOC(t) and battery temperature $\vartheta(t)$, from Eq. (14b) follows that there exist two costates, namely

$$\dot{\psi}_1^o = -\left.\frac{\partial H}{\partial SOC}\right|_o, \tag{20}$$

$$\dot{\psi}_2^o = -\left.\frac{\partial H}{\partial \vartheta}\right|_o. \tag{21}$$

For the costates, no initial conditions exist, but from Eq. (15), the end conditions

$$\psi_1^o(t_e) = 0, \tag{22}$$

$$\psi_2^o(t_e) = 0. \tag{23}$$

arise.

Even when the relations such as R_{bat}(SOC,ϑ) are assumed to be linear, hence the derivatives of the Hamiltonian are easy to calculate, no formal solution of the optimization problem could be found. The discussion of the corresponding formulas would go beyond the scope of this paper.

4.2. Application to a simplified system model

To come to a formal solution, the system model will be simplified: Although state-of-charge and battery temperature vary greatly during time, battery resistance R_{bat}(SOC,ϑ) and open-circuit voltage U_{oc}(SOC) are considered constant, neglecting the influence of SOC and ϑ over time. This simplification sacrifices accuracy in order to come a formal solution at all. At the beginning of the calculation, the parameters R_{bat} and U_{oc} will be assigned the correct value from their respective lookup table, depending on the initial values of SOC and ϑ. This correct value will be held constant during calculation. The traction power P_{trac} is also considered constant. The relation for P_{temp} given in Eq. (19) is substituted by the general $P_{temp}(\dot{Q}) = a\dot{Q}$; the corresponding value for a, a_h or a_c, will be substituted later on. Using Taylor series approximation for the battery current with different accuracy for SOC and ϑ,

$$I_{bat,SOC} = \frac{R_{bat}\left(a\dot{Q} + P_{trac}\right)^2}{U_{oc}^3} + \frac{a\dot{Q} + P_{trac}}{U_{oc}} \tag{24}$$

and

$$I_{bat,\vartheta} = \frac{a\dot{Q} + P_{trac}}{U_{oc}}, \tag{25}$$

there results a simplified system model with the equations for SOC

$$\dot{SOC}_s = -\frac{\left(R_{bat}\left(a\dot{Q} + P_{trac}\right)^2 + U_{oc}^2\left(a\dot{Q} + P_{trac}\right)\right)}{C_{nom}U_{oc}^3} \tag{26}$$

and ϑ, which discards the factor $a^2R_{bat}\dot{Q}^2$, as for the considered parameter set, $a^2R_{bat}\dot{Q} \ll U_{oc}^2$ holds:

$$\dot{\vartheta}_s = \left(\frac{\dot{Q}\left(2aR_{bat}P_{trac} + U_{oc}^2\right) + \dot{Q}_{amb}U_{oc}^2 + R_{bat}P_{trac}^2}{C_{th,bat}U_{oc}^2}\right). \tag{27}$$

The term $\lambda(\vartheta)$ is defined by

$$\lambda(\vartheta) = \lambda_0(\vartheta - \vartheta_0)^2, \tag{28}$$

with λ_0 being a constant factor and ϑ_0 the battery temperature at which least stress is applied to the battery. Eq. (28) causes the system to change the battery temperature towards ϑ_0; the more the actual battery temperature differs from ϑ_0, the more effort is taken to change it. Hence, the simplified system model has the Hamiltonian

$$\begin{aligned} H_s = &-\psi_1\frac{\left(R_{bat}\left(a\dot{Q} + P_{trac}\right)^2 + U_{oc}^2\left(a\dot{Q} + P_{trac}\right)\right)}{C_{nom}U_{oc}^3} \\ &+ \psi_2\left(\frac{\dot{Q}\left(2aR_{bat}P_{trac} + U_{oc}^2\right) + \dot{Q}_{amb}U_{oc}^2 + R_{bat}P_{trac}^2}{C_{th,bat}U_{oc}^2}\right) \\ &- \frac{\left(R_{bat}\left(a\dot{Q} + P_{trac}\right)^2 + U_{oc}^2\left(a\dot{Q} + P_{trac}\right)\right)}{C_{nom}U_{oc}^3} \\ &- w_1\lambda_0(\vartheta - \vartheta_0)^2. \end{aligned} \tag{29}$$

For the costate ψ_1^o, Eqs. (20) and (22) hold. As the parameters R_{bat} and U_{oc} are considered constant, the dependency of the Hamiltonian H_s on SOC is neglected and hence

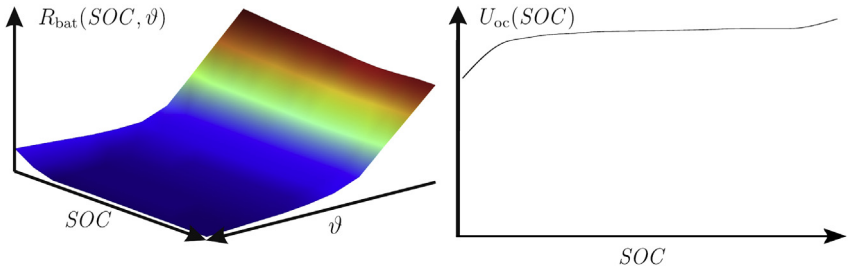

Fig. 2. Values of the parameters R_{bat} and U_{oc} used for the optimization calculations.

$$\psi_1^o(t) = 0 \quad \forall t. \tag{30}$$

Solving the necessary condition for maximizing the Hamiltonian as required by Eq. (14c),

$$\frac{\partial H_s}{\partial \dot{Q}} = 0, \tag{31}$$

for the input variable $\dot{Q}$ yields the relation

$$\dot{Q}^o = \frac{C_{nom} U_{oc} \psi_2 \left(2aR_{bat}P_{trac} + U_{oc}^2\right)}{2a^2 C_{th,bat} R_{bat}} - \frac{2R_{bat}P_{trac} + U_{oc}^2}{2aR_{bat}}. \tag{32}$$

Substituting relation (32) in the system equations and using Eq. (21) results in a coupled system of differential equations for the state ϑ^o and the costate ψ_2^o:

$$\begin{aligned} \dot{\vartheta}^o &= \psi_2^o \frac{C_{nom}\left(2aR_{bat}P_{trac} + U_{oc}^2\right)^2}{2a^2 C_{th,bat}^2 R_{bat} U_{oc}} - \frac{2R_{bat}U_{oc}^2 P_{trac} + U_{oc}^4}{2aC_{th,bat}R_{bat}U_{oc}^2} \\ &\quad - \frac{2aR_{bat}\left(R_{bat}P_{trac}^2 + U_{oc}^2 P_{trac} - \dot{Q}_{amb}U_{oc}^2\right)}{2aC_{th,bat}R_{bat}U_{oc}^2}, \\ \dot{\psi}_2^o &= 2w_1\lambda_0(\vartheta^o - \vartheta_0). \end{aligned} \tag{33}$$

The one for the SOC,

$$\dot{SOC}^o = \frac{a^2 C_{th,bat}^2 U_{oc}^2 - C_{nom}^2 \psi_2^{o2}\left(2aR_{bat}P_{trac} + U_{oc}^2\right)^2}{4a^2 C_{th,bat}^2 C_{nom} R_{bat} U_{oc}}, \tag{34}$$

is not coupled with the other two equations.

All three equations can be solved formally. The above-stated optimization problem is the one with the least simplifications for which a formal solution still could be found. Unfortunately, it suffers from some serious drawbacks: The traction power is considered constant, which means that for involving a driving cycle, it has to be split up in time periods in which the required traction power is at least nearly constant. As the costate ψ_2^o has to become 0 at the end of each period (see Eq. (23)), while its initial value is not known, the solution stringing together all time periods is not equal to the solution considering the driving cycle as a whole with changing traction power and the costate only becoming 0 at the end of the total driving cycle. Additionally, even within one period itself, the solution is not correct, as Eq. (31) does not take into account that $\dot{Q}$ is bounded. This fact results in a solution in which for example a is set to a_c because of the fact that the actual battery temperature is above ϑ_0, but the solution yields a very high heating $\dot{Q}$. This $\dot{Q}$ indeed raises the temperature even further (which is not in the sense of the objective function (16)), but as negative electric power ($a_c < 0$) is needed, said in words, produced, it charges the battery which outperforms the negative impact of the rising temperature. This is mathematically correct as the system model is given this way, but physically does not describe reality correctly. Therefore, this solution of the optimization problem is inapplicable.

4.3. Numerical solution

As a formal solution could not be found, the optimization problem will be solved numerically. The starting point is the Hamiltonian of the original system model, see Eq. (18). Using Eq. (19), the Hamiltonian for the numerical solution becomes

$$H_{num}\left(\dot{Q}\right) := \begin{cases} H|_{P_{temp}=a_h \cdot \dot{Q}} & \text{for } \dot{Q} \geq 0 \\ H|_{P_{temp}=a_c \cdot \dot{Q}} & \text{for } \dot{Q} < 0. \end{cases} \tag{35}$$

For $\lambda(\vartheta)$, Eq. (28) will be used. As $H_{num}(\dot{Q})$ is a function composed out of continuous functions, it is continuous as well, especially at $\dot{Q} = 0$, because the left-hand and right-hand limits match. In contrast to the Hamiltonian resulting from the original system model, $R_{bat}(SOC, \vartheta)$ and $U_{oc}(SOC)$ are considered constant. Fig. 18 justifies this assumption. Like in Subsection 4.2, R_{bat} and U_{oc} will be assigned the values defined by the initial state-of-charge and the initial battery temperature and held constant during time. This again leads to the conclusion

$$\psi_1^o(t) = 0 \quad \forall t. \tag{36}$$

Using Eq. (21), substituting H with H_{num}, results in

$$\dot{\psi}_2^o = -\left.\frac{\partial H_{num}}{\partial \vartheta}\right|_o = 2w_1\lambda_0(\vartheta^o - \vartheta_0). \tag{37}$$

For the calculation of the states SOC^o and ϑ^o, Eqs. (6) and (7) will be used. The input $\dot{Q}$ is determined using Eq. (14c),

$$H\left(SOC^o, \vartheta^o, \psi_1^o, \psi_2^o, \dot{Q}^o, t\right) \overset{!}{\rightarrow} \max_{\dot{Q} \in S,} \tag{38}$$

i.e., the optimal input $\dot{Q}^o$ is the particular value out of the valid set of inputs that maximizes the Hamiltonian. As a real physical system will be optimized, one has to involve that only limited tempering can be provided, $\dot{Q}_{min} \leq \dot{Q}^o \leq \dot{Q}_{max}$ with $\dot{Q}_{min} < 0$ and $\dot{Q}_{max} > 0$. Practically, $\dot{Q}^o$ is found by investigating each interval $\dot{Q}_{min} \leq \dot{Q} < 0$ and $0 \leq \dot{Q} \leq \dot{Q}_{max}$ individually. This includes checking if there is a maximum of the Hamiltonian within the interval; if there is not, check which boundary point yields the largest value for the Hamiltonian. Finally, both intervals have to be compared. This procedure of finding the optimal value corresponds to the one used in [31].

5. Results of the numerical solution

For the numerical solution, the values for $U_{oc}(SOC(t))$ and $R_{bat}(SOC(t), \vartheta(t))$ are taken from the lookup tables displayed in

Fig. 2. The considered parameter values are those of an electric vehicle lithium-ion battery; the exact numerical values cannot be released due to confidentiality. Please note that the horizontal lines coincide with the zero baseline of the vertical axes, i.e., $R_{\mathrm{bat}}(\mathrm{SOC}(t), \vartheta(t))$ and $U_{\mathrm{oc}}(\mathrm{SOC}(t))$. This means that there is a lot of variation in the data, e.g., the resistance at low temperatures is a multiple of the one at high temperatures.

Before the optimization, the exact parameter values are determined depending on the initial values of SOC and ϑ and kept constant for the rest of the calculation.

Except for the time-dependent traction power $P_{\mathrm{trac}}(t)$, all parameter values are constant. For a fixed P_{trac}, the input $\dot{Q}^{\mathrm{o}}$ depends only on the costate ψ_2^{o}; in the Hamiltonian (29), SOC does not appear and ϑ only appears in a separate summand, independent of $\dot{Q}$, and is therefore disregarded while maximizing the Hamiltonian.

For $P_{\mathrm{trac}} = 5000$ W, Fig. 3 shows the optimal system input $\dot{Q}^{\mathrm{o}}$ as a function of ψ_2^{o}.

Although this graphic displays the function for specific parameter values, it will look similar for different values of, e.g., P_{trac}: Starting from a negative ψ_2^{o}, maximum cooling power will be applied. At a certain point $\psi_{2,1}$, $\dot{Q}^{\mathrm{o}}$ jumps to or steeply rises towards $\dot{Q}^{\mathrm{o}} = 0$. At the next point, $\psi_{2,1}$, $\dot{Q}^{\mathrm{o}}$ jumps to or steeply rises towards $\dot{Q}_{\max}$. From this schematic shape, some conclusions about the general battery tempering strategy resulting from Pontryagin's maximum principle can be drawn. As the costate ψ_2^{o} has to become 0 at the end of the considered time period, the battery will not be tempered at the end of the period. Depending on the circumstances, battery tempering will be applied during some time at the very beginning. Section 6 will discuss in detail the circumstances that, among other things, determine the duration of the tempering period. The plausibility of the strategy can be illustrated by taking a look at the objective function (16). When a certain amount of electric energy for the purpose of battery tempering during the driving cycle is provided, it is reasonable to spend this energy rather early. Doing this results in a lower value for the penalty function $\lambda(\vartheta)$ which will be integrated during the remaining time. As the amount of the used electric energy is fixed, the value of

$$J_1 = \int_{t_0}^{t_{\mathrm{e}}} -\dot{\mathrm{SOC}}\,\mathrm{d}t \tag{39}$$

will be the same, no matter at which time the energy is used, whereas the value of

$$J_2 = \int_{t_0}^{t_{\mathrm{e}}} w_1 \lambda(\vartheta)\,\mathrm{d}t \tag{40}$$

will be low when the energy is used early.

The actual calculation will be carried out as follows: The coupled system of differential equations (7), (37) containing ψ_2 and ϑ will be solved simultaneously using the definition of the input $\dot{Q}^{\mathrm{o}}$, see Section 4.3. This calculation step provides the solutions for $\vartheta^{\mathrm{o}}(t)$, $\psi_2^{\mathrm{o}}(t)$ and $\dot{Q}^{\mathrm{o}}(t)$. Substituting $\dot{Q}^{\mathrm{o}}(t)$ in Eq. (6) results in an uncoupled differential equation for $\mathrm{SOC}^{\mathrm{o}}(t)$, which will be solved in the second step.

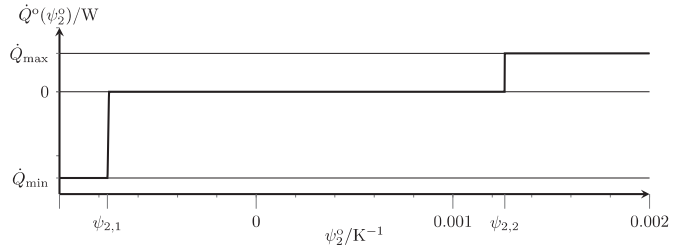

Fig. 3. The optimal system input $\dot{Q}^{\mathrm{o}}$ as a function of the optimal costate ψ_2^{o}.

Concerning the coupled system of differential equations, the question arises whether it should be solved backwards or forward in time. For ϑ^{o}, the initial temperature $\vartheta^{\mathrm{o}}(t = 0)$ is known, but its final value is not known before calculation. The costate $\psi_2^{\mathrm{o}}(t)$ only has the boundary condition (23), $\psi_2^{\mathrm{o}}(t_{\mathrm{e}}) = 0$ for its end point, while its start value is not known. As Fig. 3 shows, $\psi_2^{\mathrm{o}}(t)$ in general has quite low values, therefore its first decimals should be calculated. Additionally, it has to turn exactly to 0 at the end of the time period. In contrast, the actual initial battery temperature is determined by measurement; due to the accuracy of this measurement, it is not necessary to provide good accuracy while calculating $\vartheta^{\mathrm{o}}(t)$. Considering these facts, the system of differential equations will be solved backwards in time, starting at t_{e}. By solving it multiple times with different end temperatures, the correct initial temperature will be approached iteratively. Once the difference between calculated and measured initial temperature is within 0.01 K, the solution is accepted.

Fig. 4 shows plots of the relevant variables for a self-defined driving cycle with a duration of 250 s. As can be observed, the costate turns to 0 at the end of the cycle, giving the input $\dot{Q}^{\mathrm{o}}$ a shape according to the conclusions drawn from Fig. 3. In contrast, Fig. 5 displays the optimization results for the same driving cycle, but using only its first 50 s. In this case, the duration is so short that it does not pay off to temper the battery.

The fact that no battery tempering will be applied when the duration of the driving cycle is too short also shows that splitting up one cycle in parts of short duration and optimizing each part separately is not optimal. While optimizing the whole duration leads to battery tempering in the beginning (optimal case), optimizing each part would lead to $\dot{Q}^{\mathrm{o}} = 0$ for the whole time.

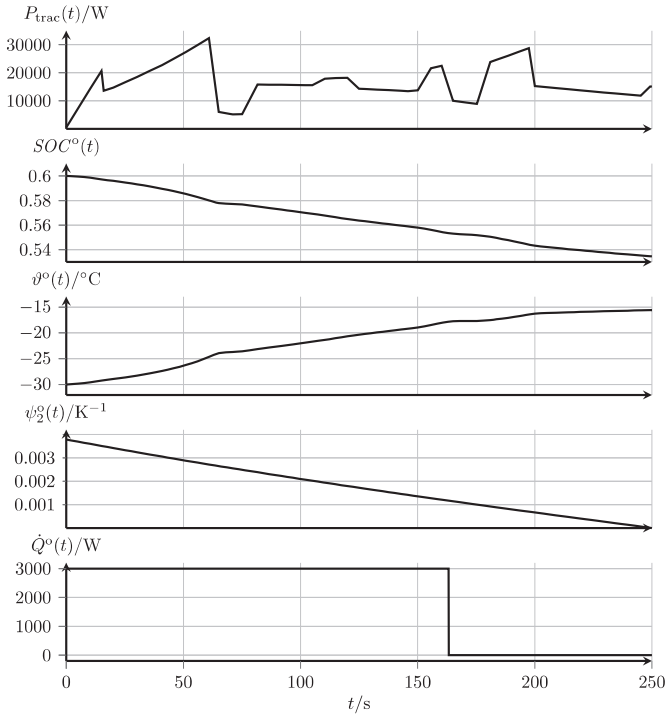

Fig. 4. Relevant variables for a driving cycle with a duration of 250 s: The first plot shows the required traction power $P_{\mathrm{trac}}(t)$. The following three ones display the course of $\mathrm{SOC}^{\mathrm{o}}(t)$, of the battery temperature $\vartheta^{\mathrm{o}}(t)$ and of the costate $\psi_2^{\mathrm{o}}(t)$, respectively, each when the optimal input $\dot{Q}^{\mathrm{o}}(t)$ (last plot) is applied.

Optimizing each interval separately and adding the objective function values results in a higher value than the objective function provides for the unsplit driving cycle optimization.

6. Causal strategy derived from the numerical solution

As the costate has to turn 0 at the end of the optimization interval, the whole driving cycle (i.e., the traction power $P_{\mathrm{trac}}(t)$) must be known in advance to be able to apply PMP. In general, this is not the case. For this reason, a causal strategy is wanted that comes close to the optimal solution, but only needs a few parameters that can be at least roughly determined in advance. Keeping in mind that only the terminal condition $\psi_2^{\mathrm{o}}(t_{\mathrm{e}}) = 0$ for the costate is available, it is necessary to determine the initial value $\psi_2^{\mathrm{s}}(t_0)$ to find a causal strategy. Note that the superscript changed from o to s, as the causal strategy will provide suboptimal results. Having found the initial value, it is possible to solve the system of differential equations (7), (37) forward in time, or, more precisely, in real-time. One method for finding the initial value will be presented in the following.

For different driving cycles, the optimization will be carried out for known conditions (initial temperature, initial state-of-charge, $P_{\mathrm{trac}}(t)$). These driving cycles include the standard driving cycles named in Table 1, but some self-defined cycles as well. The standard driving cycles cover both aggressive and gentle driving. Additional information about driving cycles can be found in [32]. Driving situations that are not suitable will not be taken into account, e.g., in some cases, the high battery resistance at low temperatures makes it impossible for the battery to provide the required power.

Figs. 6-9 show the relation between the numerically determined $\psi_2^{\mathrm{o}}(t = 0)$ and both initial temperature and initial state-of-charge (black dots). For considered periods shorter than the original cycles, only the stated duration is taken into account. At the end of this duration, the costate turns 0 and the optimization is finished.

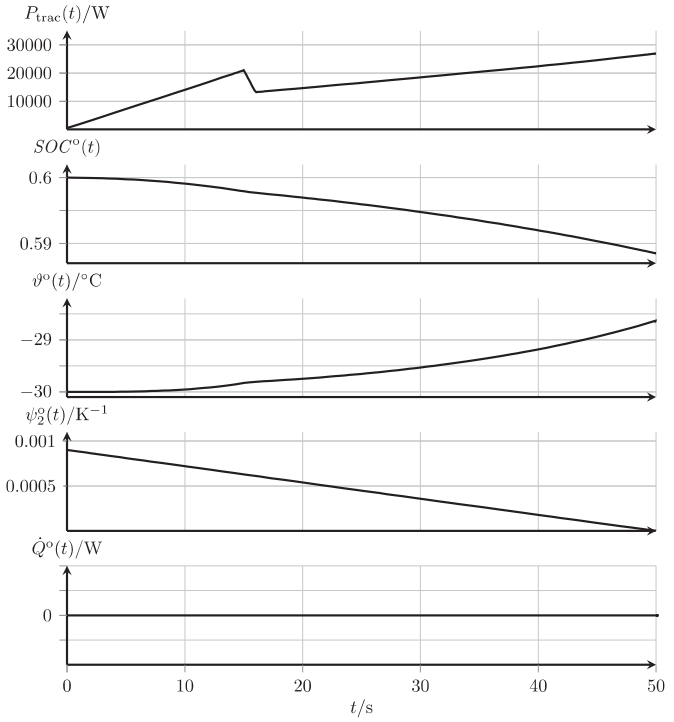

Fig. 5. Relevant variables for the first 50 s of the cycle already used in Fig. 4. Note that in case of such a short duration it is not optimal to temper the battery. As in Fig. 4, the first plot shows the required traction power $P_{\mathrm{trac}}(t)$. The following three ones display the course of $\mathrm{SOC}^{\mathrm{o}}(t)$, of the battery temperature $\vartheta^{\mathrm{o}}(t)$ and of the costate $\psi_2^{\mathrm{o}}(t)$, respectively, each when the optimal input $\dot{Q}^{\mathrm{o}}(t)$ (last plot) is applied.

Table 1
Standard driving cycles [32,33].

Driving cycle	Abbreviation	Distance/m	Duration/s	Average speed/km h^{-1}
Federal Test Procedure 72	FTP72	11,997	1369	31.6
Federal Test Procedure 75	FTP75	17,787	1874	34.2
Japanese 10-15 Mode	JPN1015 Mode	4165	660	22.7
New European Driving Cycle	NEDC	11,017	1180	33.6
New York City Cycle	NYCC	1903	598	11.5
Supplemental FTP Start Control 03	SFTPSC03	5766	596	34.8
Supplemental FTP United States 06	SFTPUS06	12,894	596	77.9
TÜV SÜD E-Car Cycle	TSECC	60,000	3600	60

Additionally, the plots include the linear approximation

$$\psi_2^{\mathrm{s}}(t = 0) = a_{\mathrm{cyc}} + b_{\mathrm{cyc}} \cdot \vartheta(t = 0) + c_{\mathrm{cyc}} \cdot \mathrm{SOC}(t = 0). \tag{41}$$

The index cyc for the parameters a, b and c only will be used when sampling points in general are named; for a particular driving cycle, it will be replaced with the cycle name. This highlights the fact that the parameter values are different for each cycle. Later on, the index will be left out when no pre-calculated sampling points are labeled, but the coefficients are used to causally determine $\psi_2^{\mathrm{s}}(t = 0)$.

For all driving cycles up to a cycle duration of about 300 s, the simulated points can be approximated quite well with the approximation (41). It can be seen from the figures that $\psi_2^{\mathrm{o}}(t = 0)$ hardly depends on $\mathrm{SOC}(t = 0)$. For this reason, c_{cyc} in Eq. (41) can be set to 0. It still will be used, though. The almost linear dependency between $\psi_2^{\mathrm{o}}(t = 0)$ and the initial temperature can be explained with Eq. (37). At a fixed cycle duration, the variation of $\psi_2^{\mathrm{o}}(t)$ depends linearly on the temperature difference $\vartheta(t) - \vartheta_0$. Because of the rather high battery heat capacity and the bounded input $\dot{Q}^{\mathrm{o}}$, battery temperature only changes slowly, therefore $\dot{\psi}_2^{\mathrm{o}}(t)$ is nearly constant and $\psi_2^{\mathrm{o}}(t)$ is almost linear. As $\psi_2^{\mathrm{o}}(t)$ has to turn 0 at the end time, the relation between $\vartheta(t = 0)$ and $\psi_2^{\mathrm{o}}(t = 0)$ is nearly linear. For increasing cycle durations, the approximation becomes more

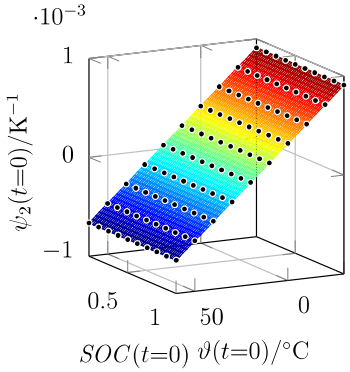

Fig. 6. The graph shows the numerically determined initial values $\psi_2^{\mathrm{o}}(t = 0)$ (black dots) depending on both initial temperature and initial state-of-charge for the JP1015Mode driving cycle with a duration of 50 s. The plot also includes the linear approximation of the dependence according to Eq. (41).

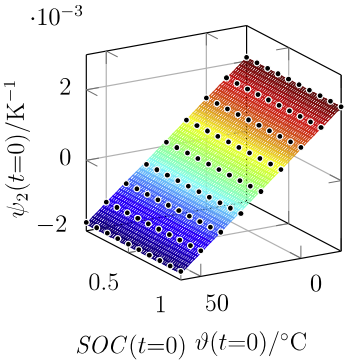

Fig. 7. The graph shows the numerically determined initial values $\psi_2^0(t=0)$ (black dots) depending on both initial temperature and initial state-of-charge for the NYCC with a duration of 150 s. The plot also includes the linear approximation of the dependence according to Eq. (41).

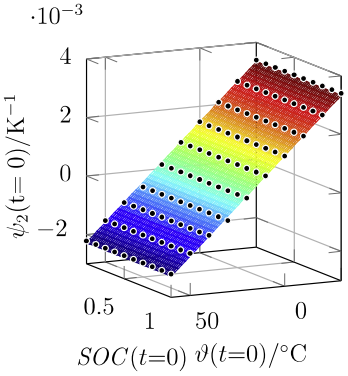

Fig. 8. The graph shows the numerically determined initial values $\psi_2^0(t=0)$ (black dots) depending on both initial temperature and initial state-of-charge for the NEDC with a duration of 200 s. The plot also includes the linear approximation of the dependence according to Eq. (41).

inaccurate, as the change in temperature becomes noticeable and $\vartheta(t)$ in Eq. (37) is not constant any more. With increasing cycle durations, the difference between simulated points and approximation first becomes bigger at points close to the optimal temperature $\vartheta_0 = 22\,°\mathrm{C}$, then at points further away from this temperature (see also Fig. 16). The impact of the battery parameters

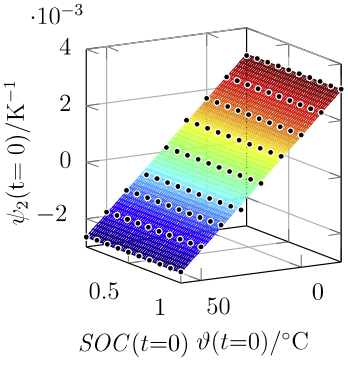

Fig. 9. The graph shows the numerically determined initial values $\psi_2^0(t=0)$ (black dots) depending on both initial temperature and initial state-of-charge for the TSECC with a duration of 250 s. The plot also includes the linear approximation of the dependence according to Eq. (41).

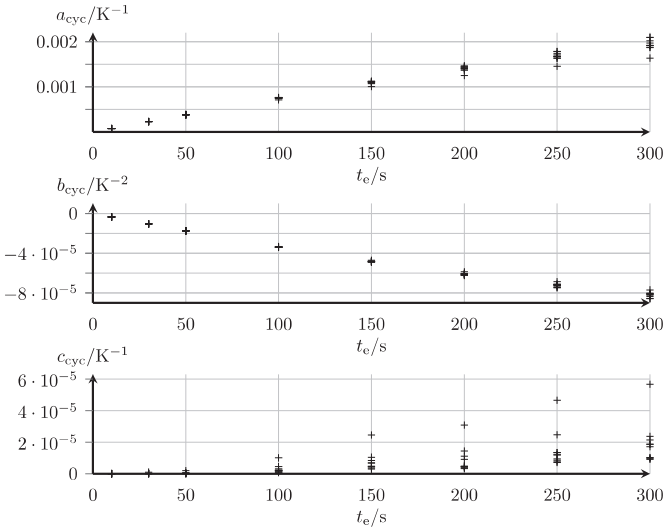

Fig. 10. For each considered cycle and cycle duration, individual values of the approximation coefficients a_{cyc}, b_{cyc} and c_{cyc} according to Eq. (41) result from the simulation runs. These three plots show all calculated values of the coefficients depending of the considered cycle duration time t_e.

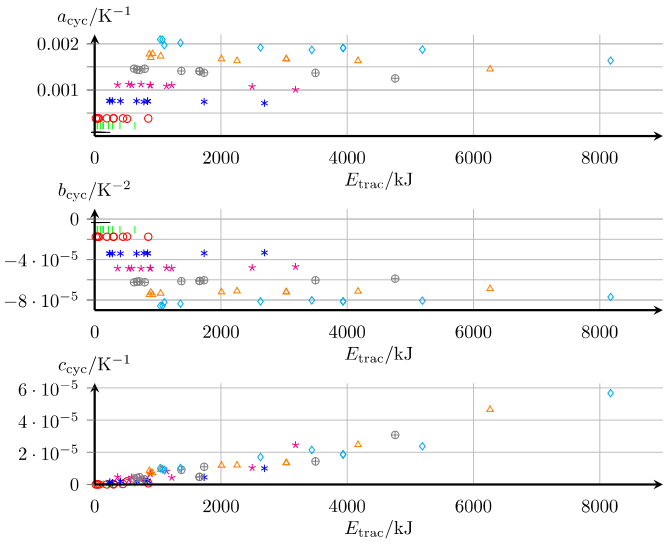

Fig. 11. The same calculated coefficients a_{cyc}, b_{cyc} and c_{cyc} as in Fig. 10 are shown here, but this time depending on the traction energy E_{trac} and not on the considered duration. Data points having the same color and mark belong to simulation runs of different driving cycles, but covering the same duration. The mark + belongs to a duration of 30 s, while cyan diamonds indicate a duration of 300 s, for instance. (For interpretation of the references to color in this figure legend, the reader is referred to the web version of this article.)

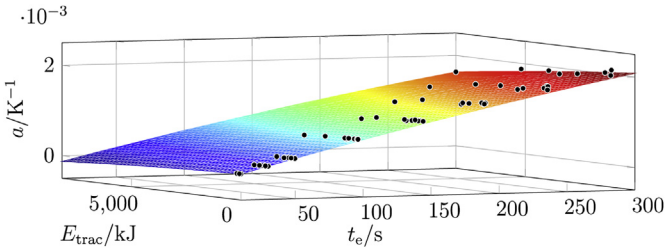

Fig. 12. a_{cyc} jointly depending on t_e (see Fig. 10) and E_{trac} (see Fig. 11) (black dots). The second-order polynomial approximation of a according to Eq. (42) is also included.

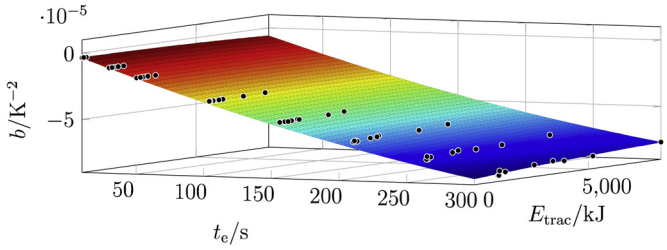

Fig. 13. b_{cyc} jointly depending on t_e (see Fig. 10) and E_{trac} (see Fig. 11) (black dots). The second-order polynomial approximation of b according to Eq. (42) is also included.

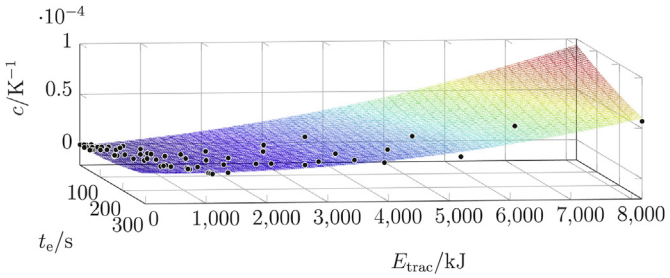

Fig. 14. c_{cyc} jointly depending on t_e (see Fig. 10) and E_{trac} (see Fig. 11) (black dots). The second-order polynomial approximation of c according to Eq. (42) is also included.

resistance and open-circuit voltage on $\psi_2^0(t = 0)$ can be neglected compared to the effect of the initial temperature.

For each driving cycle, the approximated dependency of $\psi_2^s(t = 0)$ on $\vartheta(t = 0)$ and SOC$(t = 0)$ can be expressed by the parameters a_{cyc}, b_{cyc} and c_{cyc}. These differ by the considered driving cycle. Also, they depend on the cycle duration, as already indicated by the plots in Figs. 4 and 5, respectively. In these plots, the duration of battery tempering depends on the duration of the driving cycle.

Considering Fig. 10, it becomes clear that the cycle duration is not the only parameter that determines the values of a_{cyc}, b_{cyc} and c_{cyc}. One parameter that should be investigated is the traction energy (i.e., the integral of the traction power over time), because the battery heats itself while providing the energy. This makes it necessary to provide more cooling compared to an unstressed battery at temperatures higher than ϑ_0, while at temperatures below ϑ_0, less heating is required. See Fig. 11 for the dependency of the parameters on the traction energy. Figs. 12–14 summarize the dependency of a, b and c on cycle duration and traction energy. Each plot also includes the polynomial approximation

$$x = p_{00,x} + p_{10,x}\cdot t_e + p_{01,x}\cdot E_{trac} + p_{20,x}\cdot t_e^2 + p_{11,x}\cdot t_e\cdot E_{trac} + p_{02,x}\cdot E_{trac}^2, \tag{42}$$

where x stands for one of the coefficients a, b or c. The second-degree approximation is suitable; first-degree approximation is possible, but less precise.

From Eqs. (41) and (42), the formula for the calculation of $\psi_2^s(t = 0)$ from the initial temperature $\vartheta(t = 0)$, the initial state-of-charge SOC$(t = 0)$, the expected journey time $t_{e,exp}$ and the expected traction energy that will have to be provided during the trip $E_{trac,exp}$ is

$$\begin{aligned}\psi_2^s(t = 0) = {} & \left(p_{00,a} + p_{10,a}\cdot t_{e,exp} + p_{01,a}\cdot E_{trac,exp} + p_{20,a}\cdot t_{e,exp}^2 \right.\\ & \left. + p_{11,a}\cdot t_{e,exp}\cdot E_{trac,exp} + p_{02,a}\cdot E_{trac,exp}^2\right) + \left(p_{00,b}\right.\\ & \left. + p_{10,b}\cdot t_{e,exp} + p_{01,b}\cdot E_{trac,exp} + p_{20,b}\cdot t_{e,exp}^2\right.\\ & \left. + p_{11,b}\cdot t_{e,exp}\cdot E_{trac,exp} + p_{02,b}\cdot E_{trac,exp}^2\right)\vartheta(t = 0)\\ & + \left(p_{00,c} + p_{10,c}\cdot t_{e,exp} + p_{01,c}\cdot E_{trac,exp}\right.\\ & \left. + p_{20,c}\cdot t_{e,exp}^2 + p_{11,c}\cdot t_{e,exp}\cdot E_{trac,exp}\right.\\ & \left. + p_{02,c}\cdot E_{trac,exp}^2\right)\cdot \text{SOC}(t = 0)\end{aligned} \tag{43}$$

Fig. 15 compares the acausal, optimal optimization with the causal, but suboptimal strategy. Although the costate does not exactly become 0 when the causal strategy is used, both curves are very similar. Note that the initial values $\vartheta(t = 0) = -5$ °C and

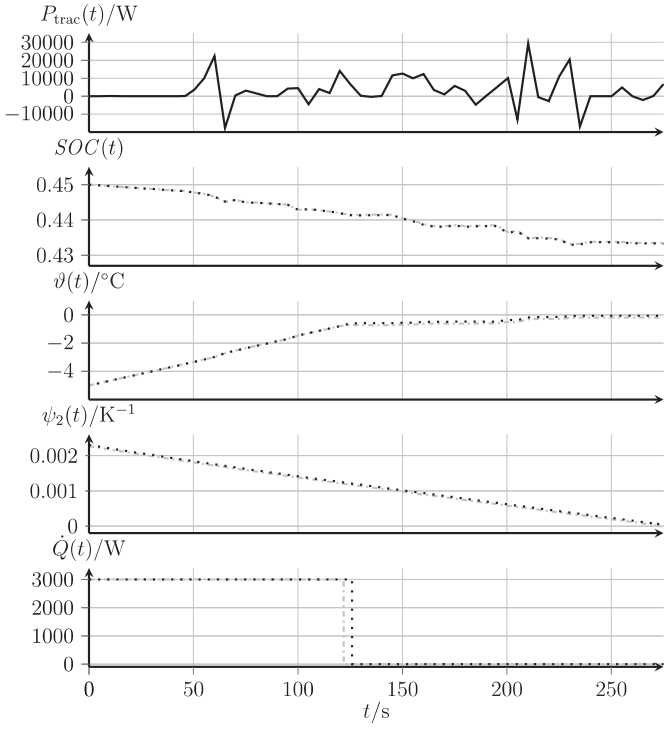

Fig. 15. Comparison between acausal, optimal (dashed/dotted gray line) and causal, suboptimal (dotted black line) optimization result. Applying the acausal optimization results in $\psi_2^0(t = t_e)$ turning to 0, while applying the causal strategy leads to a nonzero end value of ψ_2^s.

SOC$(t = 0) = 0.45$ as well as the journey time 275 s and traction energy lie between the sampling points that have been used to calculate the approximation coefficients.

Within the domain $\vartheta(t = 0) \in [-30$ °C, 60 °C], SOC$(t = 0) \in [0.1, 1]$, $t_{e,exp} \in [10$ s, 300 s], $E_{trac,exp} \in [0$ kJ, 8200 kJ], Eq. (43) is a valid approximation. For values outside the mentioned domain, it becomes inaccurate or even infeasible. Fig. 16 shows the

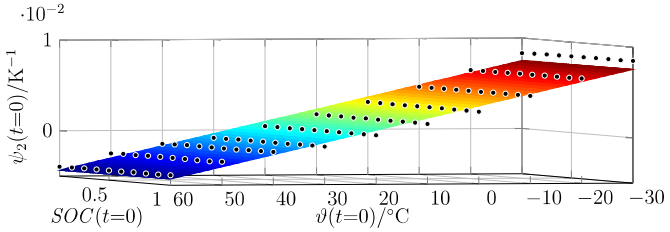

Fig. 16. Plot of the numerically determined initial values $\psi_2^0(t = 0)$, just as in Figs. 6-9. The driving cycle here is NEDC with a duration of 600 s.

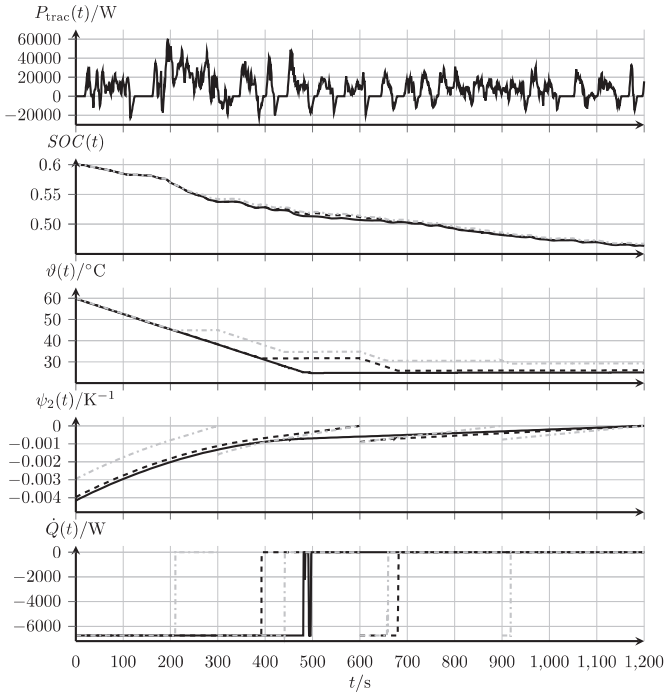

Fig. 17. Optimization of a 1200 s segment of a driving cycle (FTP75). The black line shows the optimization of the total duration, while the dashed dark gray line shows the separate optimization of periods of length 600 s, updating the parameter values after each period, according to the end values of the finished one. The dashed/dotted light gray line displays the optimization of periods of length 300 s, optimized analogously to the 600 s periods.

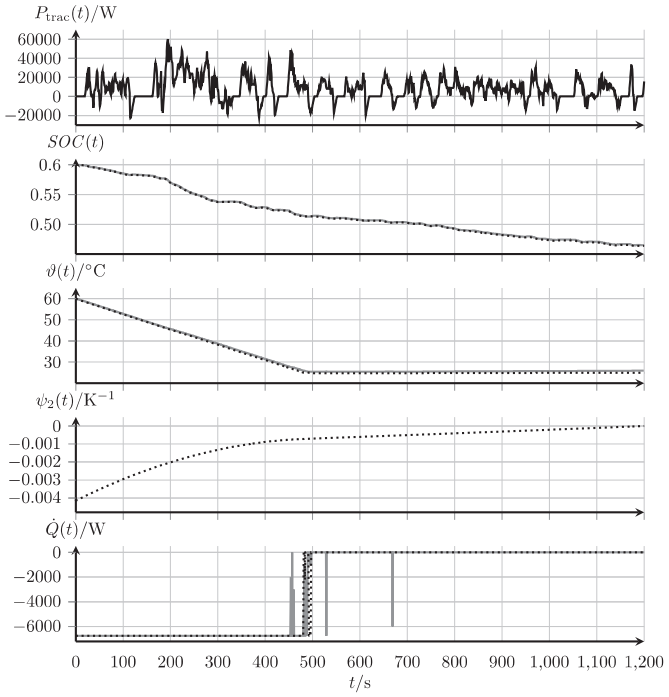

Fig. 18. Optimization of the same driving cycle segment as in Fig. 17. The dotted black line shows the optimization of the total duration with dynamic programming, whereas the gray line shows the optimization with PMP. The same traction power $P_{\mathrm{trac}}(t)$ for both optimization runs is plotted in black. The dynamic programming optimization involves updating the values for $R_{\mathrm{bat}}(\mathrm{SOC}, \vartheta)$ and $U_{\mathrm{oc}}(\mathrm{SOC})$ from the lookup table at every time step (1 s). This lookup table even takes different values for $R_{\mathrm{bat}}(\mathrm{SOC}, \vartheta)$ during charging and discharging into account. As can be seen, even for the long duration of 1200 s, the solutions hardly differ. This permits leaving the parameter values constant during each PMP optimization period.

Table 2
Final values of the objective function resulting from the optimization of a 1200 s driving cycle.

Period length	Final objective function value
1200 s	0.180707
600 s	0.184136
300 s	0.195548

initial values of ψ_2^0 for the NEDC at a duration of 600 s. In this case, the linear relation between the initial temperature and $\psi_2^0(t = 0)$ does not hold any more. Still, it is possible to use a second-order approximation similar to Eq. (42) instead of the linear one described in Eq. (41). It would then be necessary to determine 6 coefficients instead of a_{cyc}, b_{cyc} and c_{cyc}.

Fig. 17 shows a long driving cycle of 1200 s length. In addition to the acausal optimization of the whole cycle, the total duration was split in periods of 300 s and 600 s, respectively. Each period was optimized acausally, starting with the respective end values of the preceding period. The parameter values of $R_{\mathrm{bat}}(\mathrm{SOC}, \vartheta)$ and U_{oc} were updated in between the periods as well. Table 2 shows the objective function values for the three different approaches. As mentioned before, the optimization of the total duration results in the lowest, i.e., the optimal, value. Optimizing periods of 300 s provides the highest value. Fig. 17 points out that it is possible to split the total duration in periods with a maximal length of 300 s which can be optimized causally using Eq. (43), which holds true for up to 300 s. When the future driving conditions cannot be determined, it is possible to append such intervals of 300 s and optimize each of them individually with the causal approach. Alternatively, when the future driving conditions are roughly known, one can use higher approximation orders than the ones used in Eq. (43) and deduce an approximation formula for $\psi_2^s(t = 0)$ that holds for cycle durations longer than 300 s.

7. Conclusion

In this paper, Pontryagin's maximum principle (PMP) was used to find the optimal strategy to temper the battery such that it is operated in a gentle temperature range, while least electric energy is used for tempering. It was pointed out that it is not possible to come to a formal solution of the optimization problem. The numerical solution that was calculated instead was used to develop a causally applicable strategy. This causal strategy sidesteps the drawback of the PMP of only providing acausal solutions. It is only necessary to determine some general parameters of the planned journey instead of knowing the exact curve of $P_{\mathrm{trac}}(t)$ in advance. These parameters have been identified.

In Section 6, a formula was derived for a fixed parameter set that calculates the initial value $\psi_2^s(t = 0)$ of the causal costate $\psi_2^s(t)$ from the parameters initial state-of-charge, initial battery temperature, expected journey time and expected traction energy required during the journey. First, the dependence on the initial state-of-charge and the initial battery temperature was modeled linearly. In the next step, the coefficients of the linear approximation were related to the expected journey time and the expected traction energy. For different parameter sets, it might be necessary to find a more general formula

$$\psi_2^s(t = 0) = f\left(SOC(t = 0),\ \vartheta(t = 0),\ E_{\mathrm{trac,exp}},\ t_{\mathrm{e,exp}},\ \mathbf{d}\right), \tag{44}$$

where f is a suitable function and $\mathbf{d}$ is a vector that includes additional parameters that might need to be involved for different

applications. However, the causal strategy derived from the numerical solution makes it possible to draw some conclusions that are generally valid:

- By defining the penalty function (28) that punishes unfavorable battery temperature and because of the large heat capacity of the battery, there is a widely linear dependency of $\psi_2^0(t = 0)$ on the initial temperature. This dependency covers the considerable dependency of the battery resistance on the initial temperature, see Fig. 2.
- The same holds for the initial state-of-charge: Although R_{bat}(SOC, ϑ) and U_{oc}(SOC) depend on SOC in the considered case (see Fig. 2), $\psi_2^0(t = 0)$ hardly depends on SOC($t = 0$).
- The expected journey time and the expected traction energy obviously are significant parameters that must be used to approximately calculate $\psi_2^s(t = 0)$ when the detailed curve of $P_{\mathrm{trac}}(t)$ is not known. The expected journey time substantially determines whether and how long the battery needs to be tempered. The traction power provided by the battery warms it, but it is not important to know exactly how much power has to be provided at which point in time.

It is possible not to consider the traction energy (i.e., the integral of the traction power over time), but the integral of the absolute value of the traction power as parameter that needs to be involved. This is due to the fact that the battery current heats the battery, no matter if it is provided by the battery or if it flows into the battery to store recuperated energy. It has to be considered, though, that the recuperated current raises the state-of-charge, which also impacts the objective function, just like the rising battery temperature. As the dependency of $\psi_2^0(t = 0)$ on the traction energy is nonambiguous, it is reasonable to consider the traction energy rather than the integrated absolute traction power.

The development of Eq. (44), or its special case for the considered battery, Eq. (43), makes it possible to apply a strategy for battery tempering which during the trip provides a value for the objective function that comes close to the optimal one. The strategy can be implemented as follows. If the drive is already known, e.g., if it has been driven before or the destination was fed into the route guidance system, expected journey time and traction energy can be determined quite accurately. When neither the driver nor the route guidance system provides the required information, it can be determined roughly by stochastical models. From the two parameters as well as the measured initial battery temperature and the initial state-of-charge, $\psi_2^s(t = 0)$ is calculated. The differential equation (or its discrete counterpart, the difference equation) for $\psi_2^s(t)$ is then solved in real time, using the continuously measured battery temperature. From the costate and the actually measured traction power $P_{\mathrm{trac}}(t)$, the input $\dot{Q}^s(t)$ is calculated and applied.

Acknowledgments

This work was supported by a grant from the Ministry of Science, Research and Arts of Baden-Württemberg (Az: 32-720.078-1/14).

References

[1] G. Wang, Journal of Power Sources 196 (2011) 530–540.
[2] A. Khaligh, Z. Li, IEEE Transactions on Vehicular Technology 59 (2010) 2806–2814.
[3] S.J. Gerssen-Gondelach, A.P. Faaij, Journal of Power Sources 212 (2012) 111–129.
[4] C. Chan, Proceedings of the IEEE 95 (2007) 704–718.
[5] R. Cowan, S. Hultén, Technological Forecasting and Social Change 53 (1996) 61–79.
[6] E. Peled, D. Golodnitsky, H. Mazor, M. Goor, S. Avshalomov, Journal of Power Sources 196 (2011) 6835–6840.
[7] A. Burke, Proceedings of the IEEE 95 (2007) 806–820.
[8] S.B. Peterson, J. Whitacre, J. Apt, Journal of Power Sources 195 (2010) 2377–2384.
[9] L. Serrao, S. Onori, A. Sciarretta, Y. Guezennec, G. Rizzoni, in: American Control Conference (ACC), 2011, pp. 2125–2130.
[10] X. Hu, S. Li, H. Peng, Journal of Power Sources 198 (2012) 359–367.
[11] J. Wang, P. Liu, J. Hicks-Garner, E. Sherman, S. Soukiazian, M. Verbrugge, H. Tataria, J. Musser, P. Finamore, Journal of Power Sources 196 (2011) 3942–3948.
[12] V. Marano, S. Onori, Y. Guezennec, G. Rizzoni, N. Madella, in: Vehicle Power and Propulsion Conference, VPPC'09, IEEE, 2009, pp. 536–543.
[13] M. Dubarry, B.Y. Liaw, M.-S. Chen, S.-S. Chyan, K.-C. Han, W.-T. Sie, S.-H. Wu, Journal of Power Sources 196 (2011) 3420–3425.
[14] M.-J. Kim, H. Peng, Journal of Power Sources 165 (2007) 819–832.
[15] A. Jarrett, I.Y. Kim, Journal of Power Sources 196 (2011) 10359–10368.
[16] D. Gao, Z. Jin, Q. Lu, Journal of Power Sources 185 (2008) 311–317.
[17] W.-S. Lin, C.-H. Zheng, Journal of Power Sources 196 (2011) 3280–3289.
[18] D. Feroldi, M. Serra, J. Riera, Journal of Power Sources 190 (2009) 387–401.
[19] S. Kutter, B. Bäker, in: Vehicle Power and Propulsion Conference (VPPC), IEEE, 2010, pp. 1–7.
[20] M. Shams-Zahraei, A.Z. Kouzani, S. Kutter, B. Bäker, Journal of Power Sources 216 (2012) 237–248.
[21] N. Kim, A. Rousseau, D. Lee, Journal of Power Sources 196 (2011) 10380–10386.
[22] S. Stockar, V. Marano, M. Canova, G. Rizzoni, L. Guzzella, IEEE Transactions on Vehicular Technology 60 (2011) 2949–2962.
[23] L. Serrao, G. Rizzoni, in: American Control Conference, 2008, pp. 4498–4503.
[24] N. Henao, S. Kelouwani, K. Agbossou, Y. Dubé, Journal of Power Sources 220 (2012) 31–41.
[25] J. Gomez, R. Nelson, E.E. Kalu, M.H. Weatherspoon, J.P. Zheng, Journal of Power Sources 196 (2011) 4826–4831.
[26] M. Fleckenstein, O. Bohlen, M.A. Roscher, B. Bäker, Journal of Power Sources 196 (2011) 4769–4778.
[27] D. Andrea, Battery Management Systems for Large Lithium Ion Battery Packs, Artech House Publishers, 2010.
[28] L. Guzzella, A. Sciarretta, Vehicle Propulsion Systems. Introduction to Modeling and Optimization, first ed., Springer, Berlin, 2005.
[29] D. Ambühl, Energy Management Strategies for Hybrid Electric Vehicles (Ph.D. thesis), ETH Zürich, 2009.
[30] H. Geering, Optimal Control with Engineering Applications, Springer London, Limited, 2007.
[31] O. Sundström, Optimal Control and Design of Hybrid-electric Vehicles (Ph.D. thesis), ETH Zürich, 2009.
[32] T. Barlow, S. Latham, I. McCrae, P. Boulter, A Reference Book of Driving Cycles for Use in the Measurement of Road Vehicle Emissions, 2009.
[33] Auto, motor und sport, 2010. http://www.auto-motor-und-sport.de/bilder/elektroauto-reichweite-bis-zu-47-prozent-geringere-reichweite-im-winter-3295701.html?fotoshow_item=29. Online; accessed 09.07.13.